

Lightweight Hexagonal Boron Nitride Foam for CO₂ Absorption

Peter Samora Owuor,[†] Ok-Kyung Park,^{†,‡} Cristiano F. Woellner,^{†,⊥} Almaz S. Jalilov,[§] Sandhya Susarla,[†] Jarin Joyner,[†] Sehmus Ozden,^{||} LuongXuan Duy,[§] Rodrigo Villegas Salvatierra,^{§,Ⓛ} Robert Vajtai,^{†,Ⓛ} James M. Tour,^{§,Ⓛ} Jun Lou,[†] Douglas Soares Galvão,^{*,⊥} Chandra Sekhar Tiwary,^{*,†,Ⓛ} and Pulickel M. Ajayan^{*,†}

[†]Department of Material Science and NanoEngineering, Rice University, Houston, Texas 77005, United States

[‡]Department of BIN Fusion Technology, Chonbuk National University, 567 Baekje-dero, Jeonju, Republic of Korea

[§]Department of Chemistry, Rice University, Houston, Texas 77005, United States

^{||}Materials Physics and Applications Division, Los Alamos National Laboratory, Los Alamos, New Mexico 87545, United States

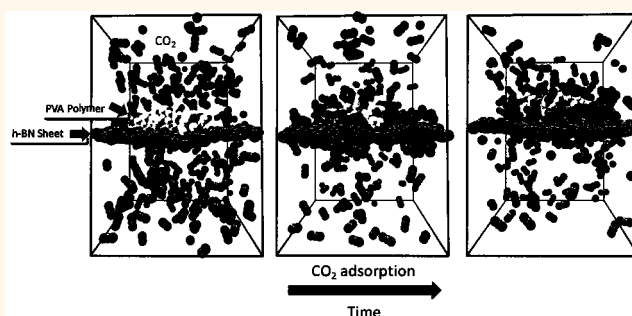
[⊥]Applied Physics Department, State University of Campinas–UNICAMP 13083-859 Campinas, SP, Brazil

Supporting Information

ABSTRACT: Weak van der Waals forces between inert hexagonal boron nitride (h-BN) nanosheets make it easy for them to slide over each other, resulting in an unstable structure in macroscopic dimensions. Creating interconnections between these inert nanosheets can remarkably enhance their mechanical properties. However, controlled design of such interconnections remains a fundamental problem for many applications of h-BN foams. In this work, a scalable *in situ* freeze-drying synthesis of low-density, lightweight 3D macroscopic structures made of h-BN nanosheets chemically connected by poly(vinyl alcohol) (PVA) molecules *via* chemical cross-link is demonstrated.

Unlike pristine h-BN foam which disintegrates upon handling after freeze-drying, h-BN/PVA foams exhibit stable mechanical integrity in addition to high porosity and large surface area. Fully atomistic simulations are used to understand the interactions between h-BN nanosheets and PVA molecules. In addition, the h-BN/PVA foam is investigated as a possible CO₂ absorption and as laser irradiation protection material.

KEYWORDS: three-dimensional materials, h-BN, CO₂ absorption, MD simulation, PVA



With its naturally occurring layered structure,¹ hexagonal boron nitride (h-BN) has emerged as an important 2D material, possessing excellent properties such as high temperature stability, high thermal conductivity, as well as mechanical strength.² Unlike its carbon graphene “cousin”, h-BN planar networks are composed of boron and nitrogen atoms arranged in a hexagonal structure, resulting in strong covalent bonds in an in-plane direction but with weak van der Waals forces between layers.^{2–4}

The fabrication of three-dimensional porous nanostructures from interconnected 2D materials such as graphene,^{3,4} clays,⁵ metal dichalcogenides,^{6,7} *etc.* has proven to be a promising technique to exploit their properties for several applications including catalysis,^{8–10} energy storage,¹¹ biological and environmental applications,¹² mechanical damping,¹³ and gas sequestration.¹⁴ Graphene and its derivatives such as graphene oxide (GO) have received much attention mainly due to their easy integration into 3D structures. The same cannot be said of few-

layer h-BN, which has proven to be difficult to synthesize as 3D constructs unless used as reinforcements¹⁵ in nanocomposites. Although chemical vapor deposition (CVD) methods,^{16,17} spark plasma welding techniques,^{18,19} and surface chemistry methods^{12,14} have achieved considerable success in designing graphene-based nanoengineered 3D structures, there still exist enormous challenges in replicating the same for h-BN structures, in particular, in large quantities for large-scale applications. Recently, the freeze-drying method^{20,21} has proved to be an efficient method to produce 3D nanostructures from their 1D or 2D constituents.^{12,13,22} This method can be improved further with surface chemistry, enabling the design of 3D structures with tailored surface properties. This combination is an inexpensive method to mass-produce selective

Received: May 12, 2017

Accepted: August 3, 2017

Published: August 3, 2017

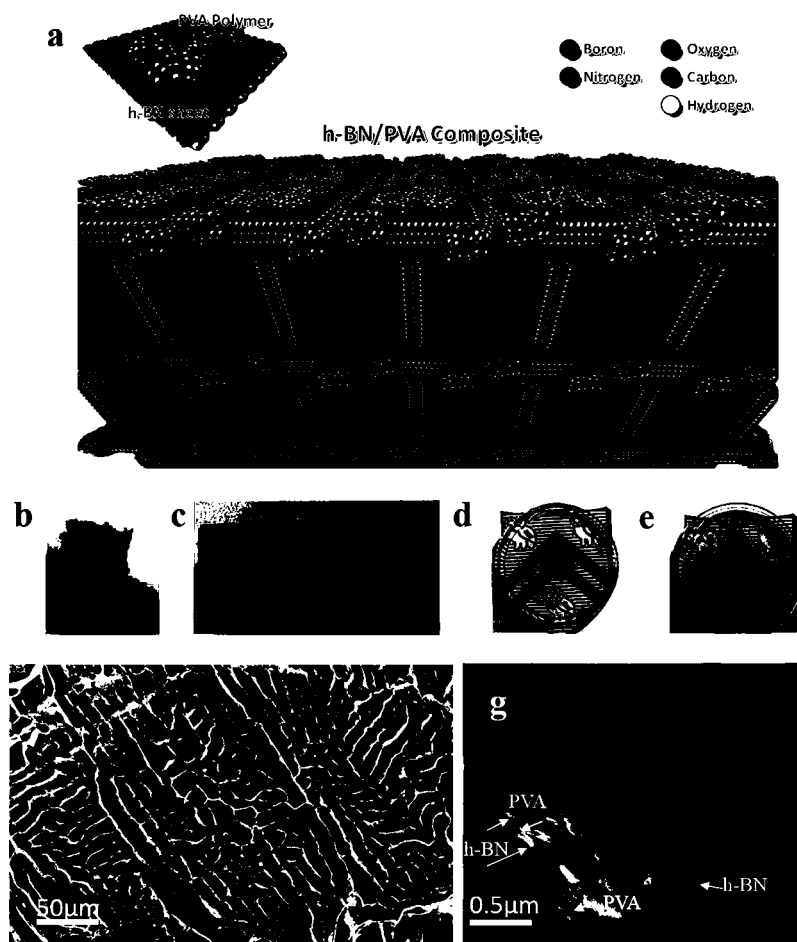


Figure 1. Characterization and morphology of h-BN/PVA foams. (a) Schematic representation depicting the h-BN nanosheets connected by poly(vinyl alcohol) (PVA) molecules. Typical chains contain 30 monomers (~ 6.2 nm chain length). The PVA molecules act like a glue to link the nanosheets through van der Waals interactions between the hydroxyl groups in the PVA and boron/nitrogen atoms in the nanosheets. (b) Structural stability of the h-BN/PVA foam. (c) Mechanical stability of the lightweight foam carrying a vial without any visible degradation. (d) Stable structure of the foam when subjected to liquids. (e) Pristine foam disintegrates in the presence of water, whereas h-BN/PVA maintains its stable interconnected morphology (Rice University owns the copyright for the logo displayed and is used with permission). (f,g) Low-magnification and high-magnification image of the foam.

macroscopic 3D nanostructures but has not been effective in producing scaffolds such as h-BN foams. 3D foams are essential for various applications due to their high porosity, hence their utilization as air filters²³ or gas absorption materials. With a controlled porosity and chemical functionalization in these 3D foams, they can serve as effective absorbents for a large class of different materials.

In this work, we report a technique to fabricate lightweight 3D macroscopic porous structures formed from h-BN nanosheets. First, the h-BN was liquid-phase-exfoliated in water to separate the layers, and then poly(vinyl alcohol) (PVA) was added (1–1.5 wt %), followed by freeze-drying. This method allows for the creation of intermolecular bonding between h-BN layers, where PVA acts like a bridge to link the individual layers, thus forming a network structure at the nanoscale. Unlike pristine h-BN foams, which normally disintegrate immediately once removed from a freeze-drier, h-BN/PVA foams show a robust freestanding structure with favorable mechanical stability. A detailed molecular dynamics (MD) study further verified and provided insights on the origins of such interconnections in improving the mechanical integrity. The foam also exhibits excellent CO₂ absorption and storage under varying pressure values. Furthermore, when coated with

polydimethylsiloxane (PDMS), the foam shows superior laser shielding properties by withstanding a varied amount of laser energy with minimal structural degradation.

RESULTS AND DISCUSSION

In Figure 1a, the proposed schematic structure of interconnected h-BN nanosheets with PVA is presented. PVA molecules act as a cross-linker to link the h-BN nanosheets. The lightweight (0.029 g/cm³), interconnected highly porous foam is shown in Figure 1b, with high mechanical stability. The foam exhibits a brown color appearance unlike the typical boron white color largely due to the PVA addition through the *in situ* freeze-drying method. The structural stability of foam is evidenced by its ability to carry a vial (2.7 g) with no visible structural damage, contrary to what is observed for pristine h-BN (Figure 1c). A major drawback of freeze-dried formed foams is their disintegration in the presence of liquids, restricting their usefulness in various applications, which can be overcome using PVA addition. We immersed a PVA-connected foam and pristine h-BN foam into water, and in less than a minute, the pristine h-BN foam broke into small pieces, unlike the interconnected h-BN/PVA foam (Figure 1d,e). The absence of interconnected networks in pristine h-BN foam

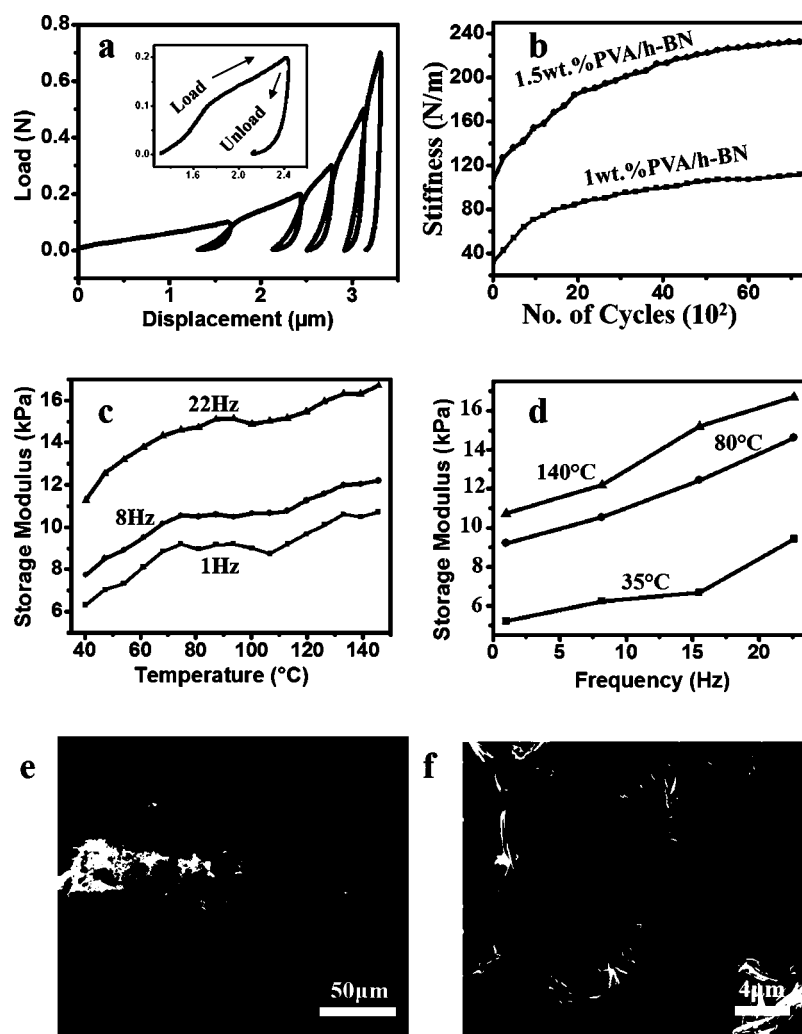


Figure 2. Mechanical response of interconnected h-BN/PVA foams. (a) Typical load–unload curves showing high structural integrity of the foams where they can sustain multiple load–unload cycles without noticeable failure. The foams can sustain loads as high as 0.7 N. (b) Self-stiffening behavior of the foam, where there is an increase in stiffness over the number of loading cycles. (c) Storage modulus vs temperature at different frequencies, with highest modulus of 15 kPa recorded at 22 Hz. (d) Storage modulus vs frequency at different temperatures. The foam is able to retain high modulus at high temperature mainly due to thermal stability of h-BN. (e) Low-magnification SEM of PVA/h-BN foam showing a network structure. (f) High-magnification SEM of PVA/h-BN foam.

could contribute to the observed structural collapse. Furthermore, the thermal stability of the h-BN is not significantly affected by the addition of PVA, as shown by the thermogravimetric analysis (TGA) thermograms (Figure S1). The low-magnification SEM images shown in Figure 1f reveal that the porous architecture of h-BN sheets is interconnected. The h-BN/PVA foam at high magnification shows that h-BN sheets are connected through thin polymer layers.

Raman spectroscopic analysis is a useful tool to obtain information on the lattice vibration modes of the foams. In Figure S2a, we present Raman spectra of h-BN and h-BN/PVA foams. For exfoliated h-BN, a characteristic Raman peak at $1366\text{--}1373\text{ cm}^{-1}$ is normally associated with the E_{2g} phonon mode.^{24,25} For the pristine h-BN foam, the Raman peak is at 1366.7 cm^{-1} with a shift of 1.5 cm^{-1} from the Raman peak of bulk h-BN (1365.2 cm^{-1}). This shift could be an indication of the reduction of the number of layers²⁶ compared to the bulk h-BN. This observation reveals an efficient exfoliation method of the pristine h-BN prior to being interconnected with PVA. On the other hand, the h-BN/PVA spectrum does not show the same h-BN characteristics. The normally low-intensity h-BN

mode disappears once the nanosheets are wetted by the PVA molecules. PVA modes become dominant in the spectrum with a mode centered at 875 cm^{-1} . X-ray diffraction data showed that the majority of crystals are normally oriented along the direction (002).⁶ This characteristic can be found at 26.7° for both h-BN and PVA interconnected foams, which is suggestive that addition of PVA does not significantly interfere with the h-BN crystallinity (see Supporting Information Figure S2b). Detailed XPS fitting was done to understand the functionalization of h-BN. The functionalization of BN sheets is evident from presence of a peak at 194 eV, resulting from the chemical shift of B 1s due to B_2O_3 . In addition to this, we also observe chemical shifts due to C–N bond in N 1s and C 1s, again indicating functionalization (see Supporting Information Figure S3). Through the oxidation reaction, hydroxyl groups ($-\text{OH}$) were formed on the surface or edge plane of BN, and the result was confirmed by Fourier transform infrared (FT-IR) spectroscopy. Comparative FT-IR spectra for raw h-BN and oxidized h-BN (f-BN) are shown in Figure S4. The broad band at 3310 cm^{-1} can be assigned to hydroxyl groups (B–OH) at the edge side of h-BN.²⁷ Furthermore, the characteristic

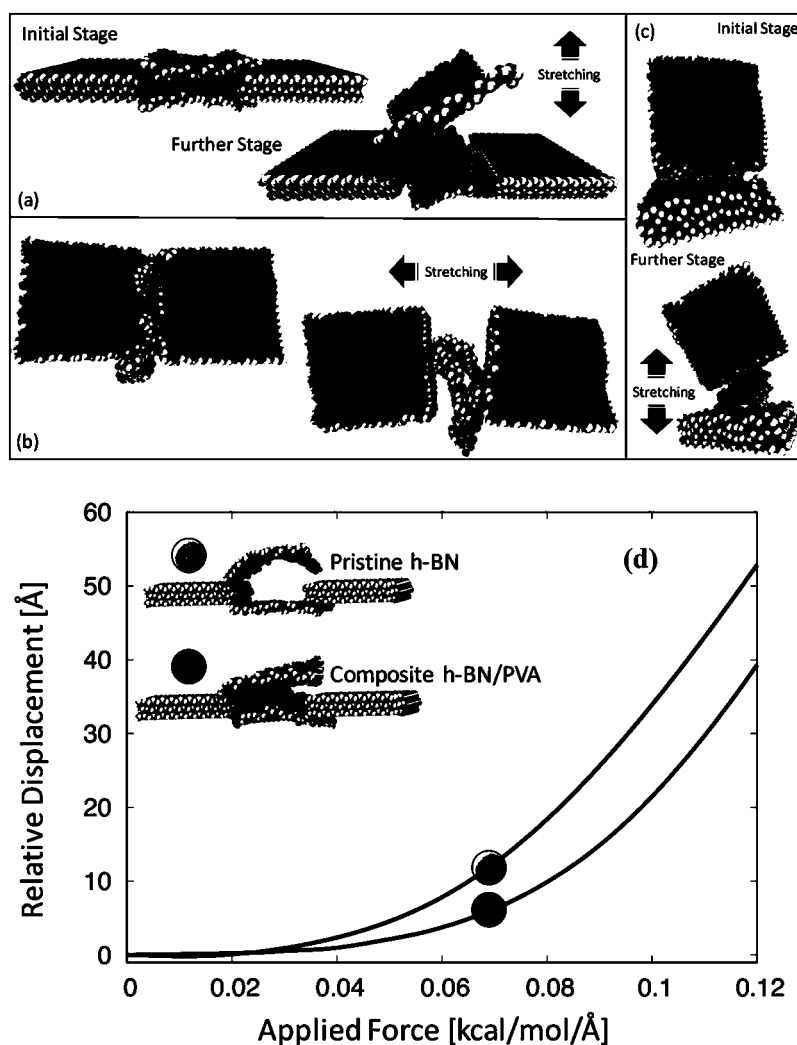


Figure 3. (Top) Snapshots of stress–strain molecular dynamics simulations for the h-BN/PVA composite comparing three different arrangements [(a) case I, (b) case II, and (c) case III] in two different stages. Initial stage shows thermalized structures at 300 K after 100 ps. The further stage snapshots show the structures under strain. All simulations were performed under a NVT ensemble. Notice the ductile-like deformation of the h-BN/PVA composite. This behavior is unlikely to happen with pristine h-BN foams. (Bottom) Relative h-BN nanosheet displacement as a function of the applied force on the upper h-BN sheets. This figure shows that the presence of the polymer (case 2) makes the composite more resilient to deformation (smaller relative displacement) when compared to the pristine h-BN structure.

peak of B–N–O appeared at 1100 cm^{-1} .²⁸ This result clearly conformed to the presence of hydroxyl groups on the surface or edge side of h-BN *via* oxidation reaction. The introduced hydroxyl groups on the surface/edge side of h-BN can form the hydrogen bond with PVA.²⁹ Furthermore, PVA can act as an effective cross-linker connecting the joints between individual h-BNs in the h-BN foam, thereby preventing slip behavior and stress concentration between the h-BN sheets and enhancing the mechanical properties of finally produced h-BN foam.^{29,30}

The interconnected h-BN/PVA foam is expected to exhibit enhanced mechanical properties. We subjected the foam to compressive loading cycles, as can be seen in Figure 2a. At low loads, the foam appears to maintain its structural integrity, unlike pristine h-BN which breaks immediately without taking any load. However, as the load increases, the foam undergoes irreversible damage. Analyzing individual load–unload cycles, we observed a nonlinear failure mechanism in the foams³¹ like those observed in metallic microlattices³² and elastomers:^{33,34} a Hookean region, a plateau, and finally densification, which is accompanied by an increase in load. Each failure region is

characterized by different failure mechanisms. For instance, linear elastic failure dominates in the Hookean region, whereas the plateau failure is due to post-buckling of the foam branches and interconnected nodes.³¹ In the densification region, as has been widely reported, the majority of internal microwalls break in large numbers without separating from each other but rather piling on top each other, which results in dense loading regions. The load–unload curves also exhibit hysteresis loops, which indicate better energy absorption. In a detailed study of h-BN foam grown by CVD, Yin *et al.*³¹ attributed these hysteresis loops to kinking and buckling of microstructures, friction between branches, and cracks developed during initial compression. Next, we monitored the change in stiffness where the foam was subjected to constant load. We observed that with a steep increase in stiffness for the initial 2000 cycles, the increase of stiffness with number of cycles does not seem to end, only reducing the rate of increasing after 2000 cycles. The interconnected foams therefore exhibit some form of self-stiffening in a dynamic load. We have reported self-stiffening behavior of a vertically grown carbon nanotube (CNT) forest

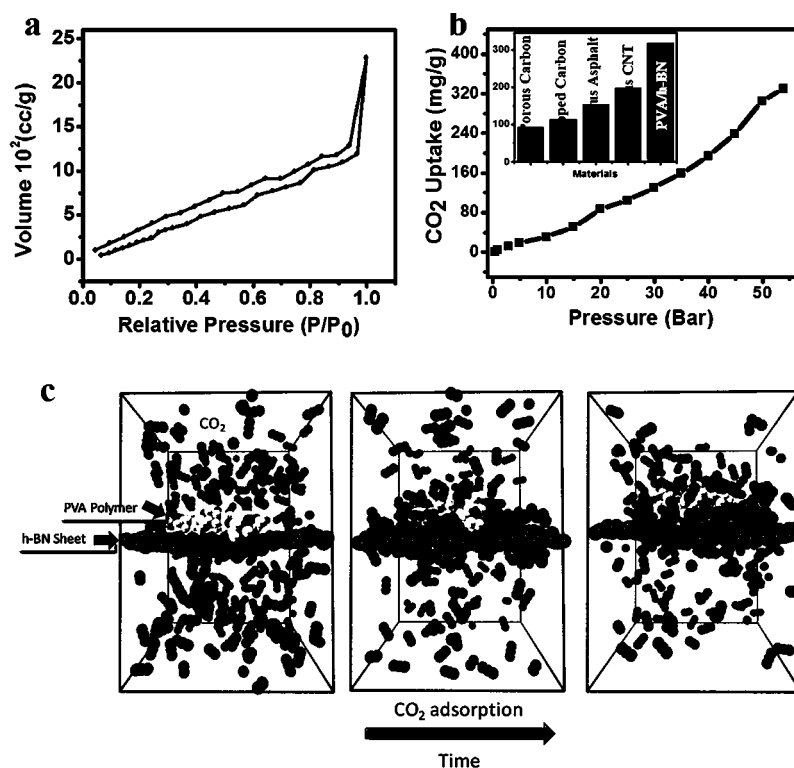


Figure 4. Surface area and CO₂ absorption of the foam. (a) Nitrogen absorption isotherm of PVA interconnected foam. (b) CO₂ uptake of the foam absorbing more than 340% of CO₂ at 65 bar and comparison with similar recently reported porous materials. (c) Snapshots (time evolution) from reactive MD simulations of the CO₂ adsorption processes (300 K during 100 ps) toward the steady state. The CO₂ adsorption observed in these snapshots is discussed in Figure 5.

and spheres³⁵ where we attributed it to chain alignment of the polymer on the CNTs.³⁶ The self-stiffening observed here could be due to well-aligned PVA molecules, which may result in a better load transfer between individual h-BN layers. In addition under dynamic load, the PVA molecules do not have enough time to relax. The fact that there is a large number of layers forming an interconnected network results in a well-distributed load within the network. However, compaction of the porous structures due to dynamic loads can also contribute to such stiffness, especially at high loads. Temperature ramp tests show a linear relationship between storage modulus and temperature (Figure 2c). The tests were carried out at different single-point frequencies, in which the storage moduli increase with an increase in temperature. The lowest modulus is observed for 1 Hz frequency and highest modulus at 22 Hz, which is double the value of that at 1 Hz. Frequency sweep tests also exhibit a linear relationship between modulus and frequency (Figure 2d). Higher modulus at high-frequency values could be attributed to the short time range the foam is given to relax. At such high frequencies, PVA molecules, which interconnect the h-BN nanosheets, do not get enough time to relax, hence the high storage modulus.

Scanning electron microscopy (SEM) was used to study the morphology of the h-BN/PVA to elucidate their inherent, enhanced mechanical properties compared to those of the pristine h-BN. As shown in Figure 2e, the foam is highly porous, forming a network-like structure. Individual h-BN nanosheets can be seen connected to each other due to the presence of PVA molecules, as clearly depicted by high-magnification SEM (Figure 2f). These types of linkages between h-BN layers is important to design such macroscopic

3D structures composed entirely of their 2D building blocks. The presence of functional groups on the edges of h-BN nanosheets provides anchoring points for the polymer molecule to join them together, thus forming very strong and stable structures. In fact, these interconnections prevent crack propagation along the whole structure by deflecting cracks once they develop within the internal structure. To further shed light on the above-mentioned observations, we carried out full atomistic molecular dynamics simulations, as discussed below.

To elucidate the role of the PVA polymer in the enhanced mechanical and structural properties of the h-BN/PVA composite, we proposed a simplified structural model depicted in Figure 1. To mimic the stress–strain response of the composite, we considered three different arrangements of h-BN sheets embedded by PVA polymer molecules. These arrangements were chosen in order to consider explicitly the interaction between the PVA polymer molecules with either the edges and the basal plane of the BN sheets. The orientations are as follows: case I (Figure 3a), two neighboring three-layer h-BN anchoring two single-layer h-BN sheets embedded with PVA; case II (Figure 3b), two neighboring three-layer h-BN with their relative edges facing each other and with PVA between; and case III (Figure 3c), rotated by 90°. Figure 3a–c presents for each considered orientation two snapshots: (initial stage) the thermalized structures, at 300 K during 100 ps and (further stage) the thermalized structures under a small strain before its complete failure. Figure 3a–c shows that the polymer makes the structures more flexible, presenting a ductile-like deformation, unlike what happens with pristine h-BN foams, which easily break apart for small loading, exhibiting a well-known brittle behavior.

To show the enhancement in the mechanical response of the h-BN/PVA composite compared to pristine h-BN foams, we carried out MD simulations comparing the force necessary to pull these two structures apart (using case I as example of arrangement), as depicted in Figure 3d. This plot shows the relative displacement of the outer h-BN sheets (center of mass) as a function of the applied time-dependent force on this h-BN sheet. This arrangement attempts to mimic the experimental conditions, and it is expected to give a reliable comparison (at least in terms of the energies involved) between the h-BN/PVA composite and the pristine h-BN foams. As evidenced in Figure 2, clearly the necessary force to pull the h-BN sheets apart is larger than in the case where the foams are filled with the PVA polymer, which results in a more resilient composite in relation to pristine h-BN foams. From the MD simulations, we can infer that the observed strong van der Waals interactions can be attributed to the high affinity between the hydroxyl groups present in PVA and h-BN nanosheets, which is consistent with the experimental observations discussed above.

Lightweight h-BN can be explored for various applications. Here, we demonstrate two uses for the h-BN/PVA, for CO₂ adsorption material and laser protection shields. For an effective CO₂ adsorption material, porosity and chemical stability are important parameters to be considered. The porosity distribution and surface area of the macroscopic h-BN/PVA foam were measured through nitrogen adsorption/desorption isotherms. As seen in Figure 4a, the curve reveals a type II adsorption/desorption isotherm for h-BN/PVA foams.³⁷ Interconnected networks formed by the PVA molecules could be responsible for such high surface areas by connecting the individual layers to an ordered porous structure.¹² The surface area of the foam has increased from 30.7 to 124.4 m²/g after 1 wt % PVA is added. The foam revealed a better pore size distribution as calculated from the Barret–Joyner–Halend (BJH) method (Figure S4). As mentioned above, porous and lightweight materials possessing high surface area are crucial for effective CO₂ absorption.^{38–40} Our h-BN/PVA foam can absorb and store CO₂ (Figure 4b). The foam captured more than 320 mg/g of CO₂ at 54 bar. This highly improved CO₂ capture and storage are attributed to the enlarged and effective surface area, ordered porosity, and presence of nitrogen atoms within the internal structure of the foam.

To further elucidate the mechanism of CO₂ adsorption in the h-BN/PVA foam, we calculated the radial distribution function (RDF) of the PVA polymer in the adsorbed h-BN layer and CO₂ in the gas phase; the structural model used in this analysis is depicted in Figure 4c (see also the video in the Supporting Information). We carried out reactive molecular dynamics simulations at room temperature (see Simulation Details section). Succinctly, RDF describes how the local time-averaged (50 ps) density varies as a function of the distance of a reference atom. To make the discussion clearer, we separated the RDF into two plots (see Figure 5), one describing the PVA polymer/h-BN sheet interactions and the other one for the CO₂ adsorbed in the PVA/h-BN composite. Figure 5a shows the RDF of the equilibrated system of the PVA polymer on top of the h-BN layer. This plot shows that both hydroxyl (black curve) and CH₃ (blue curve) groups have good affinity toward the h-BN layer, but the hydroxyl groups have stronger interactions with h-BN, in comparison to CH₃ groups, as expected. Figure 5b shows the RDF case of CO₂ gas atmosphere adsorbed into the h-BN/PVA foam. This plot

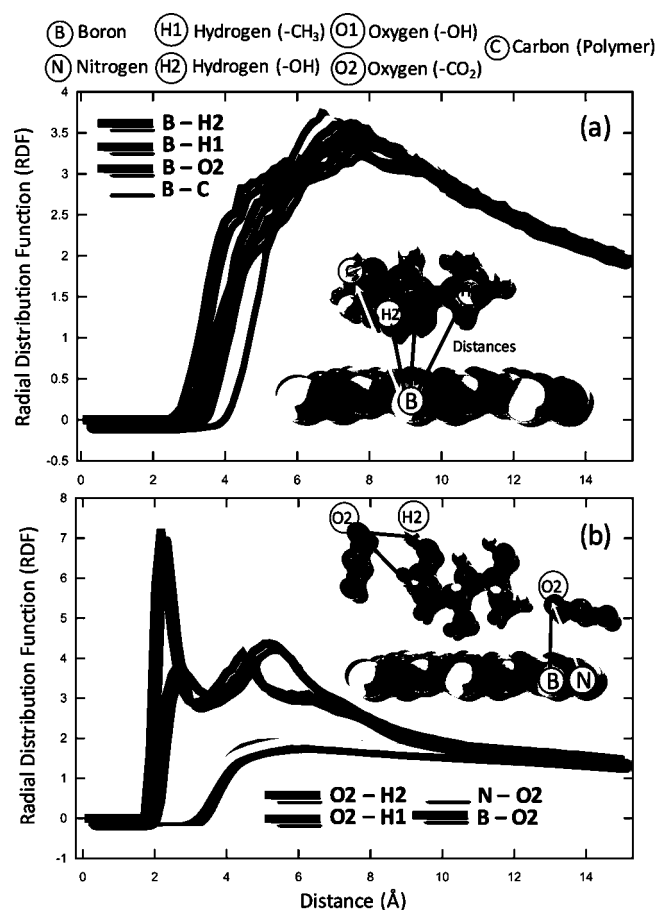


Figure 5. Radial distribution function (RDF) of (a) PVA polymer into the adsorbed h-BN layer (see Figure 1a); (b) CO₂ in the gas phase into the adsorbed PVA/h-BN composite (see Figure 4c). Results from reactive molecular dynamics simulations at 300 K. Notice the high affinity between CO₂ molecules and the PVA polymer (see text for discussion).

shows separately the CO₂ interactions with the h-BN layer (purple and green curves) and the PVA polymer (blue and red curves). CO₂ shows good affinity in both cases to the polymer and h-BN sheets. However, the CO₂ interactions with the hydroxyl and CH₃ groups presented in the PVA polymer are much stronger when compared to that of h-BN sheets, and CO₂ hydroxyl groups have the highest affinity of all.

Laser radiation damage in biological tissues is mainly due to thermal effects, where high power from the lasers leads to tissue burning and/or denaturing of proteins. With an ever-increasing power of lasers, it is important to design lightweight materials that can be used as protection shields. The thermally stable and emerging absorbing properties of low-density h-BN composite makes it good candidate for such applications. We coated our foam with PDMS to test its laser protection properties. The foam was subjected to different amounts of pulse widths with a modulation laser at 1, 10, 50, and 100% (Figure 6a) (see Experimental Section for details). To quantify the damage caused by the laser, we measured the diagonal distances for each laser energy value. As shown in Figure 6b, the damage increases with increasing laser power, though no perforation of irradiated area was observed. At low laser power, the damage is insignificant. It should be noted here that pristine h-BN foam burnt completely with a laser power less than 1%. We further imaged the irradiated areas under SEM, and as can be seen on

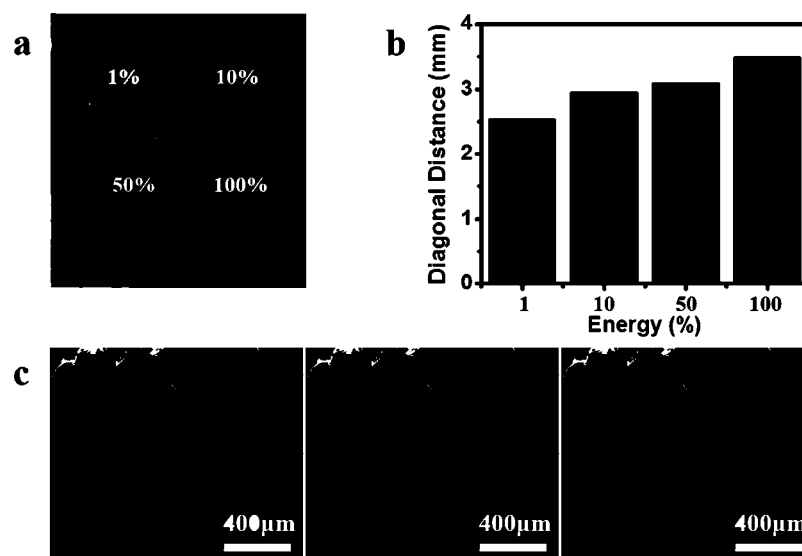


Figure 6. Foam laser irradiation resistance at different laser power values (1, 10, 50, and 100%). (a) Laser radiation does not penetrate through the sample at the irradiated areas. (b) Quantification of the effect of laser on the foam by measuring the diagonal distance on the irradiated areas; as the laser power increases, the distances increase. (c) SEM images of irradiated areas, despite the high-energy dose of the lasers; the h-BN nanosheets appear interconnected due to the presence of polymer molecules linking them together to form an interconnected lightweight structure. Magnified SEM images of the GO layers, which prevent the penetration of laser radiation through the sample.

Figure 6c, the nanosheets are still connected to each other. The interconnected networks of h-BN nanosheets prevent complete penetration of the laser energy through the foam. This interesting property could be useful for protection of laser power using this lightweight material.

CONCLUSION

In conclusion, we have reported the fabrication and mechanical characterization of stable interconnected porous lightweight h-BN foam structures. As a result of *in situ* freeze-drying with a water-soluble polymer (PVA), strong van der Waals interactions are produced among the h-BN nanosheets and the polymer, where the PVA acts like a glue to connect the sheets together. The hybrid structure exhibits enhanced mechanical properties, large surface area, and increased porosity. The interaction mechanism between the PVA and h-BN nanosheets was investigated by fully atomistic reactive MD simulations, which showed the high affinity between the hydroxyl groups present in PVA and h-BN nanosheets. Further demonstration as an efficient CO₂ absorption material (high CO₂ absorption of 340% was achieved) and laser protection is presented. A high CO₂ absorption of 340% is achieved by the foam, mainly due to nitrogen functional groups and an increased surface area.

EXPERIMENTAL SECTION

All materials and reagents used in this work were obtained from Sigma-Aldrich and used without any further treatment.

Preparation of Functionalized h-BN. For the preparation of oxidized BN (f-BN), 1 g of h-BN was dispersed in a 9:1 acid mixture (200 mL) of H₂SO₄/H₃PO₄ (99% H₂SO₄) and stirred at 50 °C for 2 h. Next, 1.5 g of KMnO₄ was added to the mixture and stirred at 50 °C for 6 h. The mixture was then poured over ice, followed by the addition of H₂O₂, and stirred for 1 h. The resulting mixtures were washed with 200 mL of DI water, 200 mL of 30 wt % HCl aqueous solution, and 200 mL of ethanol. The collected h-BN was dried at 50 °C for 24 h.

Preparation of h-BN/PVA Foam. First, 0.1 g of f-BN was added to 10 mL of DI water and sonicated for 1 h to aid in exfoliation. After sonication, the mixture was stirred at room temperature for 10 h. After

that, resorcinol (11 mM), glutaraldehyde solution (22 mM), and sodium tetraborate (0.06 mM) were added. The resulting materials were stirred for 2 h. Then, 0.1 g of 1 wt % PVA solution (solvent: DI water) was added to the BN solution, and the mixture was sonicated at room temperature for 2 h. The resulting materials were then frozen under liquid nitrogen and subsequently freeze-dried for 24 h.

Characterization. The thermal stability of h-BN/PVA foam was studied under TGA in an inert environment (argon gas, at flow rate of 100 mL/min) using a TA Instrument (Q600). Around 10–15 mg of each sample was weighed prior to testing. The samples were subjected to a temperature ramp of 10 °C/min from 30 to 700 °C.

Mechanical characterization was investigated on a dynamic mechanical analyzer (DMA, Q800 TA Instruments). All tests were done in compression mode clamps at a frequency of 1 Hz, except for frequency sweep tests where the amplitude was kept at 20 μm. Temperature ramp tests were performed from 30 to 200 °C at a heating rate of 5 °C/min. The loading condition for the stiffness test was done by applying an amplitude of 20 μm with a static force of 0.01 N while maintaining a force track of 125% on the dynamic mechanical analyzer (DMA, Q800 TA). Stiffness, storage modulus, and glass transition temperature were then obtained from the data. SEM images were taken on a FEI Quanta 400 ESEM, at a scanning electricity of 15 to 20 kV. The laser irradiation was done in air with a 10.6 μm laser (CO₂ laser) cutter system (Universal Laser System, model XLS10MWH) at a fixed frequency of 3 kHz. The laser speed was a fixed laser scribing of 15.24 cm s⁻¹ with an image density of 500 pulses per inches on an area of 0.25 cm². The laser duty cycles were varied from 1 to 100% (75 W). X-ray diffraction was done on Rigaku D/Max Ultima II with Cu Kα radiation (1.542 nm), whereas Raman measurements were done on a Renishaw Raman spectrometer with a 532 nm laser.

Simulation Details. The fully atomistic molecular dynamics simulations were performed under a NVT ensemble (at 300 K) controlled by the Nosé–Hoover thermostat, as implemented in the open source code large-scale atomic/molecular massively parallel simulator (LAMMPS).⁴¹ The fully atomistic reactive force field ReaxFF^{42,43} was used in all simulations. This force field can accurately estimate chemical reactions as bond formation and/or breaking due to its parametrization through density functional theory calculations and/or experimental data. ReaxFF uses a general relationship between bond distance/bond energy and bond order. The error in heat of formation values is around 2.8 kcal mol⁻¹, comparable to experimental data. The

time step was chosen to be 0.2 fs to ensure the numerical stability of the simulations. Our structural model system was composed of hexagonal boron nitride square sheets of 41 Å in length and PVA polymer chains made up of 30 repeating units (monomers). To simulate the stress–strain process, we first thermalized the entire system for 100 ps at 300 K, followed by an application of a time-dependent externally applied force on each boron/nitrogen atoms in the h-BN sheets along opposite directions in order to pull the sheets apart (see Figure 3d). The force was applied until the sheets broke apart. In this study, we considered three different arrangements of hexagonal boron nitride sheets covered with the PVA polymer, as described in the Results and Discussion section.

For the CO₂ adsorption simulation, we kept the same parameters and ensemble used in the stress–strain simulation. In the RDF analysis, we first equilibrated the system (depicted in Figure 4c) for 100 ps and further took the averages for another 50 ps. A video of the equilibration process can be found in the Supporting Information.

ASSOCIATED CONTENT

Supporting Information

The Supporting Information is available free of charge on the ACS Publications website at DOI: 10.1021/acsnano.7b03291.

Video S1: Effect of PVA (AVI)

Video S2: CO₂ absorption using h-BN/PVA (AVI)

Thermal stability of PVA reinforced h-BN foam; Raman spectra and XRD pattern of the h-BN/PVA; FT-IR spectra; XPS pattern; pore size distribution as calculated from the BJH method (PDF)

AUTHOR INFORMATION

Corresponding Authors

*E-mail: galvao@ifi.unicamp.br.

*E-mail: cst.iisc@gmail.com.

*E-mail: ajayan@rice.edu.

ORCID

Rodrigo Villegas Salvatierra: 0000-0001-5050-4803

Robert Vajtai: 0000-0002-3942-8827

James M. Tour: 0000-0002-8479-9328

Chandra Sekhar Tiwary: 0000-0001-9760-9768

Notes

The authors declare no competing financial interest.

ACKNOWLEDGMENTS

The authors thank the Air Force Office of Scientific Research (Grant FA9550-13-1-0084) for funding this research, and Air Force Office of Scientific Research MURI Grant FA9550-12-1-0035 financial support of this research. C.F.W. thanks São Paulo Research Foundation (FAPESP) Grant No. 2016/12340-9 for financial support. C.F.W. and D.S.G. acknowledge the Center for Computational Engineering and Sciences at State University of Campinas (FAPESP/CEPID Grant No. 2013/08293-7). S.O. acknowledges financial support from a LANL Director's Postdoctoral Fellowship.

REFERENCES

- (1) Lin, Y.; Williams, T. V.; Connell, J. W. Soluble, Exfoliated Hexagonal Boron Nitride Nanosheets. *J. Phys. Chem. Lett.* **2010**, *1*, 277–283.
- (2) Lee, K. H.; Shin, H.; Lee, J.; Lee, I.; Kim, G.; Choi, J.; Kim, S. Large-Scale Synthesis of High-Quality Hexagonal Boron Nitride Nanosheets for Large-Area Graphene Electronics Large-Scale Synthesis of High-Quality Hexagonal Boron Nitride Nanosheets for Large-Area Graphene Electronics. *Nano Lett.* **2012**, *12*, 714–718.

- (3) Chen, Z.; Ren, W.; Gao, L.; Liu, B.; Pei, S.; Cheng, H. M. Three-Dimensional Flexible and Conductive Interconnected Graphene Networks Grown by Chemical Vapour Deposition. *Nat. Mater.* **2011**, *10*, 424–428.

- (4) Chen, Z.; Xu, C.; Ma, C.; Ren, W.; Cheng, H. M. Lightweight and Flexible Graphene Foam Composites for High-Performance Electromagnetic Interference Shielding. *Adv. Mater.* **2013**, *25*, 1296–1300.

- (5) Walther, A.; Bjurhager, L.; Malho, J. M.; Pere, J.; Ruokolainen, J.; Berglund, L. A.; Ikkala, O. Large-Area, Lightweight and Thick Biomimetic Composites with Superior Material Properties via Fast, Economic, and Green Pathways. *Nano Lett.* **2010**, *10*, 2742–2748.

- (6) Zhou, J.; Huang, Y.; Cao, X.; Ouyang, B.; Sun, W.; Tan, C.; Zhang, Y.; Ma, Q.; Liang, S.; Yan, Q.; Zhang, H. Two-Dimensional NiCo₂O₄ Nanosheet-Coated Three-Dimensional Graphene Networks for High-Rate, Long-Cycle-Life Supercapacitors. *Nanoscale* **2015**, *7*, 7035–7039.

- (7) Zhou, H.; Yu, F.; Huang, Y.; Sun, J.; Zhu, Z.; Nielsen, R. J.; He, R.; Bao, J.; Goddard, W. A., III; Chen, S.; Ren, Z. Efficient Hydrogen Evolution by Ternary Molybdenum Sulfoselenide Particles on Self-Standing Porous Nickel Diselenide Foam. *Nat. Commun.* **2016**, *7*, 12765.

- (8) Wang, Z. L.; Xu, D.; Xu, J. J.; Zhang, L. L.; Zhang, X. B. Graphene Oxide Gel-Derived, Free-Standing, Hierarchically Porous Carbon for High-Capacity and High-Rate Rechargeable Li-O₂ Batteries. *Adv. Funct. Mater.* **2012**, *22*, 3699–3705.

- (9) Cai, S.; Zhang, D.; Shi, L.; Xu, J.; Zhang, L.; Huang, L.; Li, H.; Zhang, J. Porous Ni-Mn Oxide Nanosheets *In Situ* Formed on Nickel Foam as 3D Hierarchical Monolith de-NO(x) Catalysts. *Nanoscale* **2014**, *6*, 7346–7353.

- (10) Liu, Z.; Nie, H.; Yang, Z.; Zhang, J.; Jin, Z.; Lu, Y.; Xiao, Z.; Huang, S. Sulfur–nitrogen Co-Doped Three-Dimensional Carbon Foams with Hierarchical Pore Structures as Efficient Metal-Free Electrocatalysts for Oxygen Reduction Reactions. *Nanoscale* **2013**, *5*, 3283.

- (11) Rolison, D. R.; Long, J. W.; Lytle, J. C.; Fischer, A. E.; McEvoy, C. P.; Bourg, M. E.; Lubers, A. M.; Rhodes, C. P. Multifunctional 3D Nanoarchitectures for Energy Storage and Conversion. *Chem. Soc. Rev.* **2009**, *38*, 226–252.

- (12) Ozden, S.; Narayanan, T. N.; Tiwary, C. S.; Dong, P.; Hart, A. H. C.; Vajtai, R.; Ajayan, P. M. 3D Macroporous Solids from Chemically Cross-Linked Carbon Nanotubes. *Small* **2015**, *11*, 688–693.

- (13) Ozden, S.; Tiwary, C. S.; Hart, A. H. C.; Chipara, A. C.; Romero-Aburto, R.; Rodrigues, M. T. F.; Taha-Tijerina, J.; Vajtai, R.; Ajayan, P. M. Density Variant Carbon Nanotube Interconnected Solids. *Adv. Mater.* **2015**, *27*, 1842–1850.

- (14) Leonard, A. D.; Hudson, J. L.; Fan, H.; Booker, R.; Simpson, L. J.; O'Neill, K. J.; Parilla, P. A.; Heben, M. J.; Pasquali, M.; Kittrell, C.; Tour, J. M. Nanoengineered Carbon Scaffolds for Hydrogen Storage. *J. Am. Chem. Soc.* **2009**, *131*, 723–728.

- (15) Yu, Y.; Chen, H.; Liu, Y.; Craig, V. S. J.; Wang, C.; Li, L. H.; Chen, Y. Superhydrophobic and Superoleophilic Porous Boron Nitride Nanosheet/Polyvinylidene Fluoride Composite Material for Oil-Polluted Water Cleanup. *Adv. Mater. Interfaces* **2015**, *2*, 1400267.

- (16) Hashim, D. P.; Narayanan, N. T.; Romo-Herrera, J. M.; Cullen, D. A.; Hahm, M. G.; Lezzi, P.; Suttle, J. R.; Kelkhoff, D.; Muñoz-Sandoval, E.; Ganguli, S.; Roy, A. K.; Smith, D. J.; Vajtai, R.; Sumpter, B. G.; Meunier, V.; Terrones, H.; Terrones, M.; Ajayan, P. M. Covalently Bonded Three-Dimensional Carbon Nanotube Solids via Boron Induced Nanojunctions. *Sci. Rep.* **2012**, *2*, 00363.

- (17) Camilli, L.; Pisani, C.; Gautron, E.; Scarselli, M.; Castrucci, P.; D'Orazio, F.; Passacantando, M.; Moscone, D.; De Crescenzi, M. A Three-Dimensional Carbon Nanotube Network for Water Treatment. *Nanotechnology* **2014**, *25*, 065701.

- (18) Terrones, M.; Banhart, F.; Grobert, N.; Charlier, J. C.; Terrones, H.; Ajayan, P. M. Molecular Junctions by Joining Single-Walled Carbon Nanotubes. *Phys. Rev. Lett.* **2002**, *89*, 75505.

- (19) Ozden, S.; Brunetto, G.; Karthiselva, N. S.; Galvão, D. S.; Roy, A.; Bakshi, S. R.; Tiwary, C. S.; Ajayan, P. M. Controlled 3D Carbon

Nanotube Structures by Plasma Welding. *Adv. Mater. Interfaces* **2016**, *3*, 1500755.

(20) Vinod, S.; Tiwary, C. S.; Machado, L. D.; Ozden, S.; Vajtai, R.; Galvao, D. S.; Ajayan, P. M. Synthesis of Ultralow Density 3D graphene–CNT Foams Using a Two-Step Method. *Nanoscale* **2016**, *8*, 15857–15863.

(21) Vinod, S.; Tiwary, C. S.; da Silva Autreto, P. A.; Taha-Tijerina, J.; Ozden, S.; Chipara, A. C.; Vajtai, R.; Galvao, D. S.; Narayanan, T. N.; Ajayan, P. M. Low-Density Three-Dimensional Foam Using Self-Reinforced Hybrid Two-Dimensional Atomic Layers. *Nat. Commun.* **2014**, *5*, 4541.

(22) Koizumi, R.; Hart, A. H. C.; Brunetto, G.; Bhowmick, S.; Owuor, P. S.; Hamel, J. T.; Gentles, A. X.; Ozden, S.; Lou, J.; Vajtai, R.; Asif, S. A. S.; Galvao, D. S.; Tiwary, C. S.; Ajayan, P. M. Mechano-Chemical Stabilization of Three-Dimensional Carbon Nanotube Aggregates. *Carbon* **2016**, *110*, 27–33.

(23) Tang, B.; Zhang, L.; Li, R.; Wu, J.; Hedhili, M. N.; Wang, P. Are Vacuum-Filtrated Reduced Graphene Oxide Membranes Symmetric? *Nanoscale* **2016**, *8*, 1108–1116.

(24) Lin, Y.; Williams, T. V.; Xu, T. B.; Cao, W.; Elsayed-Ali, H. E.; Connell, J. W. Aqueous Dispersions of Few-Layered and Monolayered Hexagonal Boron Nitride Nanosheets from Sonication-Assisted Hydrolysis: Critical Role of Water. *J. Phys. Chem. C* **2011**, *115*, 2679–2685.

(25) Gorbachev, R. V.; Riaz, I.; Nair, R. R.; Jalil, R.; Britnell, L.; Belle, B. D.; Hill, E. W.; Novoselov, K. S.; Watanabe, K.; Taniguchi, T.; Geim, A. K.; et al. Hunting for Monolayer Boron Nitride: Optical and Raman Signatures. *Small* **2011**, *7*, 465–468.

(26) Bhimanapati, G. R.; Kozuch, D.; Robinson, J. Large-Scale Synthesis and Functionalization of Hexagonal Boron Nitride Nanosheets. *Nanoscale* **2014**, *6*, 11671–11675.

(27) Hou, J.; Li, G.; Yang, N.; Qin, L.; Grami, M. E.; Zhang, Q.; Wang, N.; Qu, X. Preparation and Characterization of Surface Modified Boron Nitride Epoxy Composites with Enhanced Thermal Conductivity. *RSC Adv.* **2014**, *4*, 44282–44290.

(28) Sudeep, P. M.; Vinod, S.; Ozden, S.; Sruthi, R.; Kukovec, A.; Konya, Z.; Vajtai, R.; Anantharaman, M. R.; Ajayan, P. M.; Narayanan, T. N. Functionalized Boron Nitride Porous Solids. *RSC Adv.* **2015**, *5*, 93964–93968.

(29) Zeng, X.; Ye, L.; Yu, S.; Li, H.; Sun, R.; Xu, J.; Wong, C. P. Artificial Nacre-like Papers Based on Noncovalent Functionalized Boron Nitride Nanosheets with Excellent Mechanical and Thermally Conductive Properties. *Nanoscale* **2015**, *7*, 6774–6781.

(30) Qi, X.; Yang, L.; Zhu, J.; Hou, Y.; Yang, M. Stiffer but More Healable Exponential Layered Assemblies with Boron Nitride Nanoplatelets. *ACS Nano* **2016**, *10*, 9434–9445.

(31) Yin, J.; Li, X.; Zhou, J.; Guo, W. Ultralight Three-Dimensional Boron Nitride Foam with Ultralow Permittivity and Superelasticity. *Nano Lett.* **2013**, *13*, 3232–3236.

(32) Torrents, A.; Schaedler, T. A.; Jacobsen, A. J.; Carter, W. B.; Valdevit, L. Characterization of Nickel-Based Microlattice Materials with Structural Hierarchy from the Nanometer to the Millimeter Scale. *Acta Mater.* **2012**, *60*, 3511–3523.

(33) Gibson, L. J. Modelling the Mechanical Behavior of Cellular Materials. *Mater. Sci. Eng., A* **1989**, *110*, 1–36.

(34) Gibson, L. J.; Ashby, M. F.; Zhang, J.; Triantafillou, T. C. Failure Surfaces for Cellular Materials under Multiaxial Loads—I. Modelling. *Int. J. Mech. Sci.* **1989**, *31*, 635–663.

(35) Owuor, P. S.; Tiwary, C. S.; Koizumi, R.; Soto, M.; Hart, A. H. C.; Barrera, E. V.; Vajtai, R.; Lou, J.; Ajayan, P. M. Self-Stiffening Behavior of Reinforced Carbon Nanotube Spheres. *Adv. Eng. Mater.* **2017**, *19*, 1600756.

(36) Carey, B. J.; Patra, P. K.; Ci, L.; Silva, G. G.; Ajayan, P. M. Observation of Dynamic Strain Hardening in Polymer Nanocomposites. *ACS Nano* **2011**, *5*, 2715–2722.

(37) Esteves, I. A. A. C.; Cruz, F. J. A. L.; Muller, E. A.; Agnihotri, S.; Mota, J. P. B. Determination of the Surface Area and Porosity of Carbon Nanotube Bundles from a Langmuirian Analysis of Sub- and Supercritical Adsorption Data. *Carbon* **2009**, *47*, 948–956.

(38) Bae, Y.; Snurr, R. Q. Minireviews Development and Evaluation of Porous Materials for Carbon Dioxide Separation and Capture. *Angew. Chem., Int. Ed.* **2011**, *50*, 11586–11596.

(39) Casco, M. E.; Martinez-Escandell, M.; Silvestre-Albero, J.; Rodriguez-Reinoso, F. Effect of the Porous Structure in Carbon Materials for CO₂ Capture at Atmospheric and High-Pressure. *Carbon* **2014**, *67*, 230–235.

(40) D'Alessandro, D. M.; Smit, B.; Long, J. R. Carbon Dioxide Capture: Prospects for New Materials Angewandte. *Angew. Chem., Int. Ed.* **2010**, *49*, 6058–6082.

(41) Plimpton, S. Fast Parallel Algorithms for Short-Range Molecular-Dynamics. *J. Comput. Phys.* **1995**, *117*, 1–19.

(42) Van Duin, A. C. T.; Dasgupta, S.; Lorant, F.; Goddard, W. A. ReaxFF: A Reactive Force Field for Hydrocarbons. *J. Phys. Chem. A* **2001**, *105*, 9396–9409.

(43) Chenoweth, K.; Cheung, S.; Van Duin, A. C. T.; Goddard, W. A.; Kober, E. M. Simulations on the Thermal Decomposition of a Poly(dimethylsiloxane) Polymer Using the ReaxFF Reactive Force Field. *J. Am. Chem. Soc.* **2005**, *127*, 7192–7202.